Live-cell imaging of exocyst links its spatiotemporal dynamics to various stages of vesicle fusion

Felix Rivera-Molina and Derek Toomre

Department of Cell Biology, Yale University School of Medicine, New Haven, CT 06510

Tethers play ubiquitous roles in membrane trafficking and influence the specificity of vesicle attachment. Unlike soluble *N*-ethyl-maleimide–sensitive fusion attachment protein receptors (SNAREs), the spatiotemporal dynamics of tethers relative to vesicle fusion are poorly characterized. The most extensively studied tethering complex is the exocyst, which spatially targets vesicles to sites on the plasma membrane. By using a mammalian genetic replacement strategy, we were able to assemble fluorescently tagged Sec8 into the exocyst complex, which was shown to be functional by biochemical, trafficking, and morphological criteria. Ultrasensitive live-cell imaging revealed that Sec8-TagRFP moved to the cell cortex on vesicles, which preferentially originated from the endocytic recycling compartment. Surprisingly, Sec8 remained with vesicles until full dilation of the fusion pore, supporting potential coupling with SNARE fusion machinery. Fluorescence recovery after photobleaching analysis of Sec8 at cell protrusions revealed that a significant fraction was immobile. Additionally, Sec8 dynamically repositioned to the site of membrane expansion, suggesting that it may respond to local cues during early cell polarization.

Introduction

Tethering factors play important roles in membrane traffic. At many different trafficking steps, they provide an initial long-distance interaction between the vesicle and target membrane that can influence the fidelity of vesicle delivery, upstream of SNARE-mediated fusion (Sztul and Lupashin, 2009; Bröcker et al., 2010; Yu and Hughson, 2010). One of the most extensively studied tethering factors is the exocyst, an octomeric protein complex composed of Sec3/5/6/8/10/15/Exo70/84 proteins that targets vesicles to specific sites on the plasma membrane (PM; Heider and Munson, 2012; Liu and Guo, 2012). In budding yeast, where exocyst proteins were first identified (Novick et al., 1980), the exocyst is required for vesicle targeting to the bud tip and cleavage furrow (TerBush et al., 1996). Specifically, Sec15 is anchored to the vesicle through the Rab GTPase Sec4, whereas Sec3 and Exo70 act as "spatial landmarks" on the PM for complex assembly (Finger et al., 1998) or polarity (Heider and Munson, 2012). In mammalian cells, perturbation of the exocyst (using blocking antibodies, overexpressed mutants, or RNAi) revealed that it is essential in a myriad of cellular processes, such as cell division, secretion, migration, and ciliogenesis and formation of junctions, invadopodia, and nanotubes (Liu and Guo, 2012; Heider and Munson, 2012).

Although the exocyst has the molecular interactions (Munson and Novick, 2006) and physical size (Hsu et al., 1998) to bridge the vesicle to the PM, precisely how it is linked in space and time to vesicle fusion is not understood. This is because the exocyst (or any other tether) has not been directly observed relative to vesicle fusion. Biochemical assays provide a means to dissect vesicle tethering from fusion and have shown that two multisubunit tethers (HOPS and TRAPP) bind vesicles to their target (Cai et al., 2007; Stroupe et al., 2009), but these ensemble techniques cannot provide the temporal and spatial information to fully elucidate the tethering process.

A key open question regarding exocyst dynamics is when and where are exocyst components recruited and released. In mammalian cells it has been speculated that three subunits (Sec10/Sec15/Exo84) ride on the vesicle and assemble with the other subunits at the PM (Moskalenko et al., 2003; Wu et al., 2008), a concept that is at odds with results in budding and fission yeast whereby most or all subunits are bound to the vesicle (Finger et al., 1998; Boyd et al., 2004; Bendezú et al., 2012). It has also been speculated that the exocyst, given its large size (~750 kD), may need to be removed in order for the vesicle to

Correspondence to Derek Toomre: derek.toomre@yale.edu

Abbreviations used in this paper: IP, immunoprecipitation; KD, knockdown; PM, plasma membrane; ROI, region of interest; TIRFM, total internal reflection fluorescence microscopy.

The Rockefeller University Press $30.00
J. Cell Biol. Vol. 201 No. 5 673–680
www.jcb.org/cgi/doi/10.1083/jcb.201212103

get close enough to the PM to fuse (Heider and Munson, 2012). Yet many multisubunit tethers, including the exocyst, interact with the SNARE machinery (Sivaram et al., 2005; Yu and Hughson, 2010; Morgera et al., 2012), suggesting that they may be linked to the fusion step. Although biochemical and genetic data have shown interactions between the exocyst and SNAREs (Wiederkehr et al., 2004; Grosshans et al., 2006), this binding could either stabilize the interaction of the tether to the acceptor compartment, promote vesicle fusion, or both (Bröcker et al., 2010).

Dynamic imaging of tethers relative to vesicle exocytosis would be a direct means to elucidate the orchestration of tethering and fusion. Unfortunately, current methods cannot probe the transitory nature of tethers. Exocyst subunits were systematically tagged with GFP in MDCK cells a decade ago, but most GFP fusions produced diffuse cytosolic labeling, incongruent with localization to vesicles (Matern et al., 2001). However, in budding yeast, imaging and photobleaching studies showed that triple GFP–tagged subunits moved on puncta into the bud tip (Boyd et al., 2004). This was not studied in relationship to vesicle tethering or fusion, which may be technically challenging because of the rapid flux and high density of vesicles in the yeast bud. Exocyst subunits have also been imaged in fission yeast (Bendezú and Martin, 2011), *Arabidopsis thaliana* (Pecenková et al., 2011), *Dictyostelium discoideum* (Essid et al., 2012), and *Drosophilia melanogaster* (Guichard et al., 2010), but it is not clear if the probes were bona fide reporters of the exocyst complex.

To study the role of the exocyst in constitutive exocytosis, we combined a genetic replacement strategy to label the exocyst with a fluorescently tagged version of Sec8 in mammalian cells with sensitive imaging of vesicle arrival and fusion by total internal reflection fluorescence microscopy (TIRFM). We show that Sec8 arrived on recycling vesicles and surprisingly remained until full dilation of the fusion pore, indicating a potential link with the SNARE fusion machinery. In live migrating cells, Sec8 dynamically repositioned to sites where membrane outgrowth subsequently occurred, suggesting that it may act during early stages of cell polarization.

Results and discussion

Genetic replacement strategy to study exocyst dynamics in mammalian cells

It has been shown that GFP-tagged exocyst subunits mislocalize to the cytosol when expressed in MDCK cells; an exception was Exo70-GFP, yet its overexpression decreased transepithelial resistance (Matern et al., 2001). Although a trivial explanation is that the tags rendered the subunits nonfunctional, another is that most overexpressed GFP-tagged subunits were not incorporated into the complex. We favor the latter possibility. First, in yeast most GFP-tagged exocyst subunits genetically rescued ts phenotypes (Boyd et al., 2004). Additionally, single particle studies of the conserved oligomeric Golgi subcomplex, a tethering complex with subunits structurally similar to the exocyst, showed that most GFP-tagged subunits were assembled in the complex (Lees et al., 2010).

We designed experiments to test whether a fluorescently tagged exocyst subunit will become incorporated into the holocomplex if its endogenous counterpart is selectively knocked down. We observed that exogenous Sec8 tagged at the C terminus with TagRFP (rSec8-TagRFP) was partially degraded in HeLa cells at low expression and further degraded at higher expression (Fig. 1 A). In contrast, when endogenous Sec8 was simultaneously depleted (~80% knockdown [KD] efficiency; Fig. 1 A, lane 1 vs. 7) and rescued with RNAi-resistant rat Sec8-TagRFP, the tagged Sec8 became more stable, especially at low expression (0.1 µg), with levels similar (~98%) to endogenous Sec8 in control cells (Fig. 1 A, lane 8 vs. 1). Immunoprecipitated (IP) rSec8-TagRFP was able to pull down other exocyst subunits in Sec8KD cells (Fig. 1 B), supporting that it was incorporated into the functional complex.

We next performed the corresponding imaging experiments. In control cells, overexpressed rSec8-TagRFP appeared either cytosolic (Fig. 1 C, asterisk) or in large aggregates (arrows), as reported previously (Matern et al., 2001). In striking contrast, when Sec8 was knocked down, rSec8-TagRFP appeared as dim diffraction-limited puncta by TIRFM (Fig. 1 C, right). Live-cell movies (Video 1) and corresponding kymographs (Fig. 1 D) revealed that small (<250 nm) Sec8 puncta moved into the evanescent field, stayed in a fixed position (<500 nm xy displacement), and then rapidly disappeared (Fig. 1 D, arrowheads). The size and dynamics of Sec8 spots are consistent with a putative vesicle tether at the PM. Importantly, these dim, dynamic punctae were only observed when endogenous Sec8 was knocked down and only by using sensitive live TIRFM cell imaging (and not by confocal microscopy; unpublished data).

Sec8 arrives on vesicles that tether to the PM and fuse

To test if the appearance of Sec8 at the surface corresponded to vesicle tethering, "Sec8-replaced" cells were cotransfected with Vamp2-GFP (a type II membrane protein); Vamp2 was chosen because it is involved in trafficking pathways that interface with the exocyst in adipocytes (Kanzaki and Pessin, 2003). As seen in Video 2 and its maximum projection image in Fig. 2 A, many peripheral Vamp2-GFP spots colocalized with rSec8-TagRFP (arrows). The corresponding kymograph (Fig. 2 B) revealed that rSec8-TagRFP puncta appeared and disappeared concurrently with Vamp2-GFP puncta (open and closed arrowheads, respectively); the bright static Vamp2-GFP structures that were negative for Sec8 may represent endosomes or clathrin patches on the PM. The lifetime of rSec8-TagRFP spots (n = 3,000 objects) showed a median duration of ~7.5 s (Fig. 2 C). Imaging of deeper TIRFM (>300-nm penetration depth) indicated that Sec8 was on vesicles, as many of the small puncta exhibited long-range motion along curvilinear paths, which is consistent with trafficking along microtubules (Fig. S1 A and Video 2). Additional analysis of rSec8-TagRFP colocalization with other vesicle markers (Fig. S1, C and D) showed a high colocalization with the recycling endosome marker Rab11 (~60%) but only ~20% colocalization with the post-Golgi markers VSVG and NPY (Fig. 2 D). Nearer to the cell surface (~150-nm penetration depth), rSec8-TagRFP appeared with the arrival of Vamp2-GFP vesicles (Fig. 2 E, open arrowhead) and disappeared when the vesicles fused (closed arrowhead). Sometimes Vamp2-GFP rapidly brightened (Fig. 2 E, asterisk;

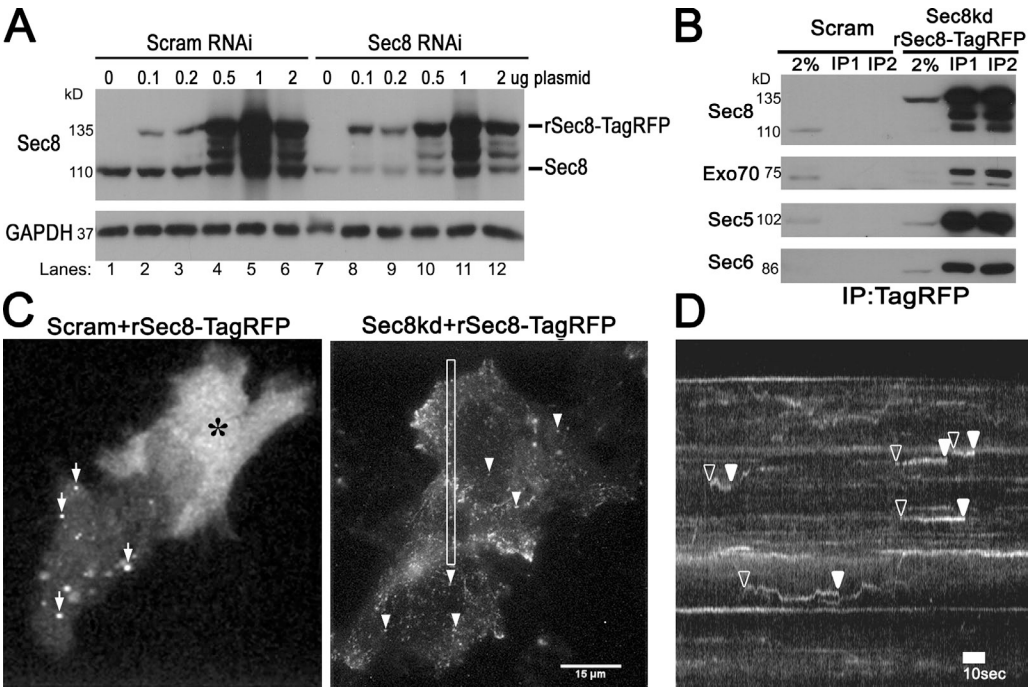

Figure 1. **KD and replacement of endogenous Sec8 enables rSec8-TagRFP to be incorporated into the exocyst and visualization of small dynamic puncta by TIRFM.** (A) HeLa cells were transfected with rSec8TagRFP and either scrambled (Scram) RNAi or RNAi to Sec8 for 60 h and immunoblotted against Sec8, which showed that rSec8-TagRFP was stabilized after Sec8KD. (B) IP of TagRFP pulled down other exocyst subunits in "Sec8-replaced" stable cells (Sec8KD plus rSec8TagRFP). (C) Live-cell TIRFM showed that rSec8-TagRFP localized to small dot-like structures in Sec8-replaced cells. (left) Cells transfected with Scram RNAi and rSec8-TagRFP showed aggregates (arrows) or cytoplasmic localization (asterisk). (right) KD rSec8-TagRFP in Sec8-replaced cells showed vesicle-like structures (arrowheads; maximum projection of Video 1). (D) Kymograph of box in C. rSec8-TagRFP puncta appeared (open arrowheads), remained static, and disappeared (closed arrowheads), indicative of potential tethering.

and Fig. S1 B, trace) a few seconds before its exocytic release, which may correspond to either the opening of the fusion pore (as lumenal GFP is slightly acid quenched) or an axial movement of the vesicle before fusion. As this assignment was difficult, we later turned to the highly pH-sensitive GFP variant pHluorin to better monitor vesicle fusion. Nonetheless, these results provide direct evidence that the components of the exocyst are present on vesicles that arrive and tether at the PM. It should be noted that our findings are incongruent with a mammalian model in which Sec8 resides on a PM subcomplex (Moskalenko et al., 2003; Wu et al., 2008); rather, they agree with yeast studies indicating that Sec8 is on the vesicle (Boyd et al., 2004).

Sec8 remains localized until full expansion of the fusion pore

To better address the kinetics of Sec8 relative to vesicle fusion and identify the origin of Sec8-positive vesicles we used pHluorin-tagged cargo. As shown in the maximum-intensity projection (Fig. 3 A) and in Video 3, about half of the Vamp2-pHluorin fusion events had rSec8-TagRFP associated with them (Fig. 3 A, yellow arrowheads and circles). In several cells the colocalization was pronounced in the cell periphery (Fig. 3 A, white arrows), consistent with the view that the exocyst promotes fusion at specific PM sites (Rossé et al., 2006; Letinic et al., 2009).

Using pHluorin, we were able to unambiguously identify the initial opening of the fusion pore, as Vamp2-pHluorin rapidly (within a frame) brightened because of de-acidification of the vesicle with the neutral extracellular milieu (Fig. 3 B, asterisk). Strikingly, the Sec8 signal did not disappear at the opening of the fusion pore, but instead persisted until the vesicle fully fused, as assayed by measuring the lateral diffusion of Vamp2 into the PM (Xu et al., 2011). This indicates that Sec8 remains at fusion sites until the cargo disperses into the PM. We next imaged the release of pHluorin-tagged transferrin receptor (TfRc-pH; Fig. 3 B, second panel). To obtain a quantitative temporal profile of Sec8 recruitment, we temporally aligned 120 rSec8-TagRFP traces to the moment of fusion (based on the TfRc-pH spike; Fig. 3 C, dashed line) and then averaged them. The resulting Sec8 intensity profile showed three features: (1) a rising phase before fusion, (2) a peak just before vesicle fusion, and (3) a decay phase with kinetics virtually identical to the diffusional loss of TfRc-pH. These distinct results strongly suggest that an exocyst component is associated with the vesicle until fusion is complete. Thus, our dynamic molecular imaging of Sec8 indicates that vesicle tethering is coordinated not only with the initial moment of fusion, but also with the later stage of fusion pore dilation.

Exocyst vesicles emanate from recycling endosomes

The origin of the vesicles that use the exocyst is unclear as exocyst components have been reported to regulate the delivery of both post-Golgi vesicles (Grindstaff et al., 1998; Grosshans et al., 2006) and recycling endocytic vesicles to the PM (Prigent et al., 2003; Langevin et al., 2005; Zárský and Potocký, 2010). In epithelial cells, the exo- and endocytic circuits may cross, as post-Golgi cargo can traverse exocyst-positive recycling endosomes

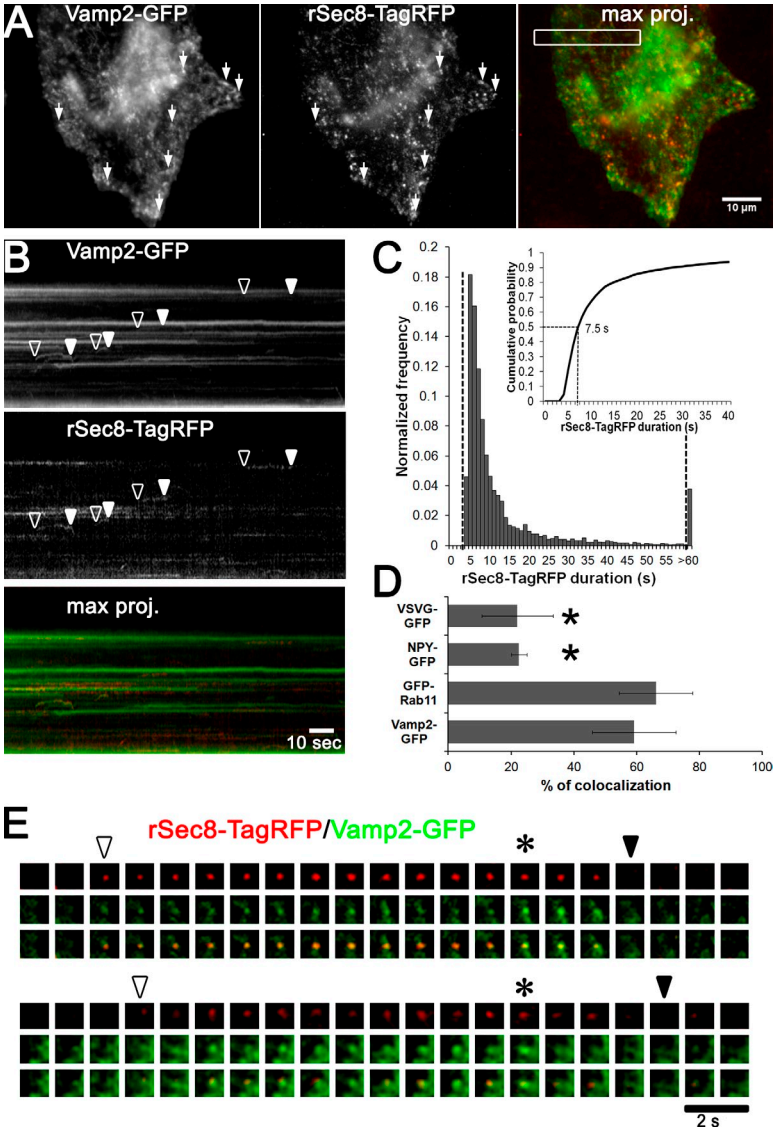

Figure 2. **Dynamics of the exocyst rSec8-TagRFP trafficking on vesicles.** (A) HeLa cells were knocked down for Sec8, co-transfected with Vamp2-GFP/rSec8-TagRFP, and imaged by TIRFM at 2 Hz. Maximum projections (5 min) were generated (Video 2; arrows show colocalization). (B) Kymograph of box in A shows the appearance and disappearance of vesicles (arrowheads). (C) Track length measurements (~3,000) were made to determine the median duration (~7.5 s) of rSec8-TagRFP (histogram; inset shows cumulative probability graph). (D) rSec8-TagRFP colocalization analysis with post-Golgi cargos (VSVG-GFP and NPY-GFP) or recycling endosomes markers (GFP-Rab11 and Vamp2-GFP). $n = 4$ cells per cargo; error bars = SD; *, P = 0.001, *t* test. (E) Two galleries of a dual labeled vesicle show the appearance (open arrowhead) and disappearance (closed arrowhead) of vesicles at the PM. Asterisks show when the Vamp2-GFP intensity increases.

en route to the basolateral surface (Fölsch et al., 2003; Ang et al., 2004). Our results in Fig. 2 D show that the majority of Rab11-containing vesicles (~65%) colocalized with the exocyst, unlike post-Golgi cargo (~20%) . To directly determine to which extent prototypic recycling and post-Golgi cargo use the exocyst, we compared the colocalization of TfRc (a bona fide recycling marker) and a pulsed-released post-Golgi exocytic cargo with rSec8-TagRFP during vesicle fusion; both cargos were tagged with pHluorin on their extracellular side. As shown earlier, many TfRc (and Vamp2)-containing vesicles that underwent fusion co-localized with Sec8, but some did not (Fig. 3 A, green arrowheads). Quantification of 260 TfRc-pH fusion events revealed that ~50% of them were associated with a Sec8 signal (Fig. 3 D). As transferrin receptor can also recycle through a "short" route via sorting endosomes, exocyst-negative vesicles may originate from these compartments. As a post-Golgi cargo we generated a secreted protein and TfRc containing four FM aggregation domains and a lumenal pHluorin (ssFM4-pH and TfRcFM4-pH); FM4 retains cargo in the ER until AP21988 (2 µM) is added, after which time the cargo can come out as a wave to the surface (Rivera et al., 2000; see Fig. S2 A). After 30-min incubation with the ligand, only ~20% of ssFM4-pH or TfRcFM4-pH fusion events colocalized with Sec8, indicating that most post-Golgi carriers in nonpolarized cells do not use the exocyst. This minor colocalization may be reconciled if a portion of the post-Golgi carriers passed en route to the surface through the recycling compartment, as shown in epithelial cells (Fölsch et al., 2003; Ang et al., 2004). In contrast, after 120-min treatment with the AP21988, which allowed TfRcFM4-pH to recycle through endosomes to the cell surface, the colocalization with Sec8 increased to ~50%.

Consistent with a major role of the exocyst in the endocytic recycling pathway, and as a third functional assay for rSec8-TagRFP, we observed that Sec8KD caused an approximately fourfold increase in the perinuclear accumulation of transferrin-Alexa568 (Fig. S2 C, normalized to transferrin receptor) relative to control KD cells (Fig. S2 D, asterisk). This recycling block was fully rescued by expressing rSec8-tagRFP (Fig. S2 D, double asterisk). Together with the biochemical and live-cell imaging assays, these results support that rSec8-tagRFP is functional and that vesicles emanating from recycling endosomes use the

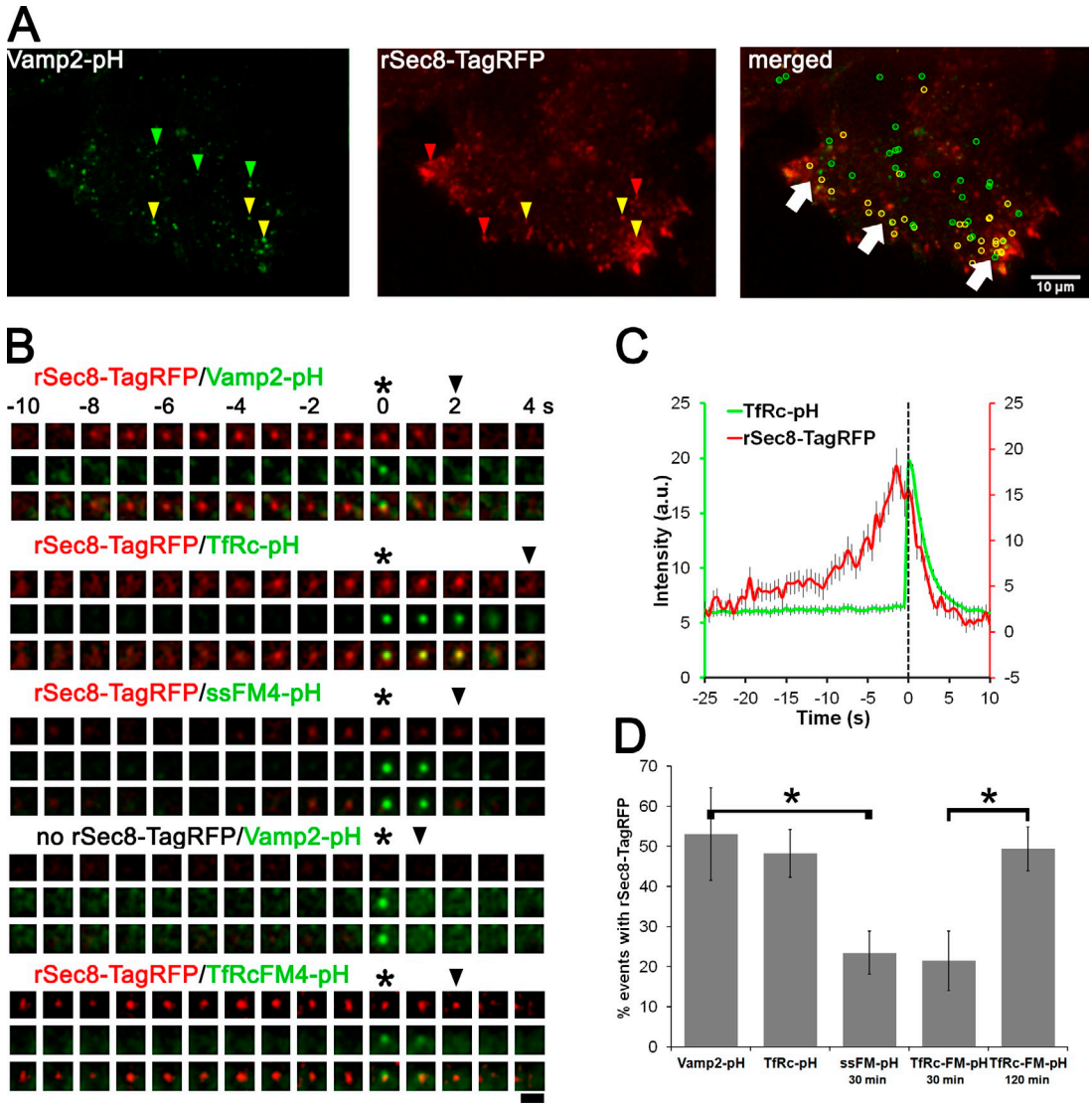

Figure 3. **Exocyst rSec8-TagRFP colocalized with endosomal vesicles and remained until full dilation of the fusion pore.** (A) Cells treated with Sec8 RNAi and cotransfected with Vamp2-pHluorin (Vamp2-pH) and rSec8-TagRFP were imaged by TIRFM (5 min at 2 Hz). Maximum projection images are shown (Video 3). Vamp2-pHluorin fusion events that colocalize with rSec8-TagRFP are shown as yellow arrowheads and circles; noncolocalizing events are in green and red. White arrows show regions of extensive colocalization in the cell periphery. (B) Galleries of single vesicle fusion of rSec8-TagRFP and different pHluorin (pH) cargos: Vamp2, TfRc, and post-Golgi releasable soluble cargos ssFM4-pH and TfRcFM4-pH. Asterisks and arrowheads show when the fusion pore opens and vesicles fully fuse, respectively. Bar, 2 µm. (C) 120 fusion events were temporally aligned by fusion pore opening and merged (error bars = SEM). (D) Quantification of the percentage of fusion events that contained rSec8-TagRFP for the four cargos. n = 5–8 cells per cargo; 243–428 events/condition; error bars = SD; *, P = 0.001, t test.

exocyst, in agreement with previous findings (Prigent et al., 2003; Langevin et al., 2005; Oztan et al., 2007).

Exocyst vesicles dynamically mark the site of membrane expansion.

We noticed that in living cells rSec8-TagRFP was frequently seen in bright patches adjacent to protrusions (Figs. 1 C and 4 A), consistent with exocyst localization in fixed cells (Rosse et al., 2009; Andersen and Yeaman, 2010). To address the kinetics of Sec8 recruitment to protrusions, we performed FRAP experiments in combination with TIRFM imaging. Rapid bleaching of rSec8-TagRFP in protrusions (Fig. 4 A) showed that many puncta appeared to move into the bleached region and then disappear (Video 4), as indicated by the curvilinear tracks on multiline kymograph (Fig. 4 A, bottom). FRAP analysis revealed that the recovery, after correcting for minor photobleaching, could be fitted by a single exponential with a half-time of ∼40 s (Fig. 4 B; n = 5 cells). Notably, about one third (32.5%) of Sec8 in cell protrusions was in a nonrecoverable immobile fraction. In yeast, however, it was reported that there was no immobile fraction because ∼40% recovery could be observed after bleaching ∼66% of total exocyst at the bud tip (Boyd et al., 2004). In our case the rSec8-TagRFP signal in the box shown in Fig. 4 A before FRAP only accounted for 6% of the total fluorescence; thus even after correcting for the bleached fraction, ∼26% of Sec8 was immobile. A potential ramification is that an immobile pool of exocyst may act as a local signaling hub and/or spatial cue as postulated previously (He and Guo, 2009).

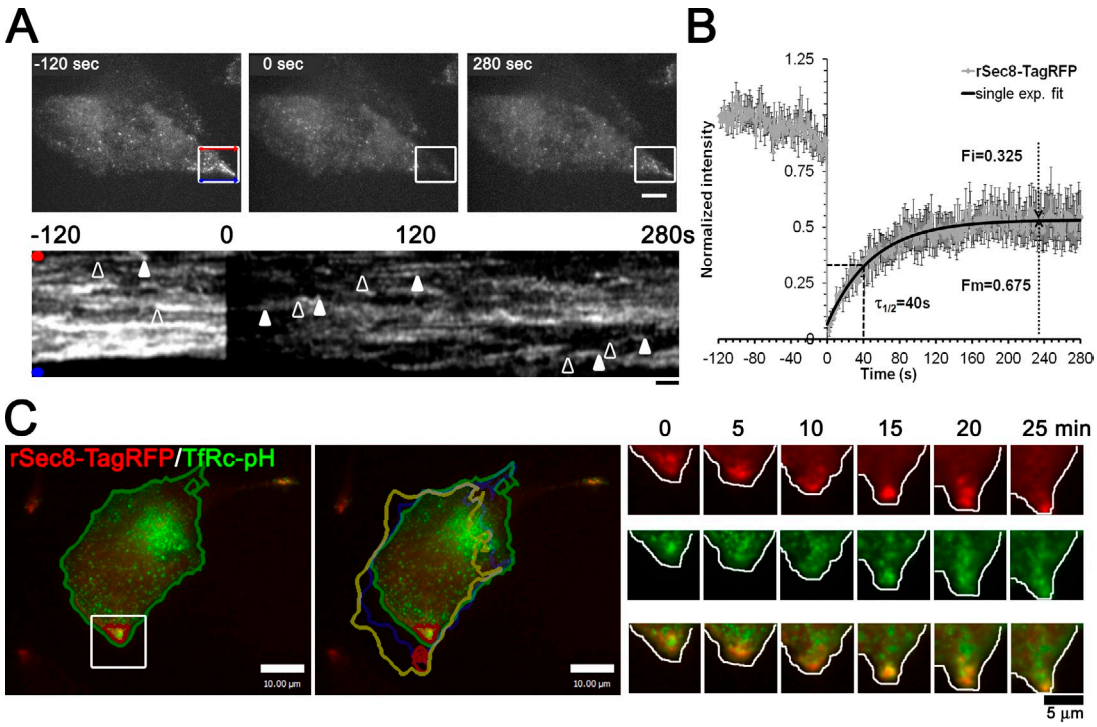

Figure 4. **Exocyst rSec8-TagRFP is highly dynamic on cell protrusions and accumulates in clusters at the leading edge during cell migration.** (A) Images of rSec8-TagRFP dynamics at cell protrusions by TIRFM/FRAP (see Video 4). Images of rSec8-TagRFP in stable Sec8-replaced HeLa cells in which a ROI is photobleached at time 0 s; kymographs of the ROI are shown beneath. Arrowheads show the appearance and disappearance of rSec8-TagRFP tracks. (B) ROI signal corrected for photobleaching (n = 5; error bars = SEM) fits to a single exponential (black line) and was used to calculate the half-time of recovery ($\tau_{1/2}$), mobile fraction (F_m), and immobile fraction (F_i). (C) rSec8-TagRFP dynamics at the leading edge of migrating cells by dual color TIRFM. (left) Images of a stable EA hy926 cell (Sec8KD/rSec8-TagRFP) transfected with TfRc-pH show the cell position at time 0 (green) and at 30 min (yellow). A gallery of the ROI is on the right. rSec8-TagRFP accumulated where the cell subsequently moved (see Video 5).

To monitor the dynamics of Sec8 relative to vesicle traffic and polarized membrane expansion we imaged rSec8-TagRFP in migrating human endothelial cells (EA hy926); supplemental experiments validated the KD of Sec8 and replacement with rSec8-TagRFP (Fig. S3 A). Similar to HeLa cells, rSec8-TagRFP was found in protrusions and colocalized with TfRc-pH fusion events (Fig. S3 B). Remarkably, in the course of 30 min, as the cell turned and repositioned itself toward the bottom of the field of view, fluorescent exocyst punctae were continuously seen near the leading edge, where membrane expansion occurred (Fig. 4 C and Video 5). Together with our FRAP analysis, these results suggest that the exocyst may act as a local hub that can dynamically respond during early stages of cell polarization (Liu and Guo, 2012).

In summary, our combined genetic replacement and imaging approach indicates that an exocyst component (Sec8) is in the right place at the right time to contribute to the tethering of recycling endocytic vesicles. Moreover, this tether remains until SNARE-mediated fusion is completed. Because many multisubunit tethering complexes can interact with SNARES, they may serve to proofread SNARE assembly or promote fusion (He and Guo, 2009; Yu and Hughson, 2010; Heider and Munson, 2012). For the yeast exocyst, Sec6 interacts with both Sec9 (a SNAP-25 orthologue; Sivaram et al., 2005) and Sec1 (a Munc18 orthologue or SM protein; Morgera et al., 2012) but not both simultaneously. Intriguingly, SM proteins are known to play a key role in fusion pore expansion (Vardjan et al., 2013). Moreover VPS33, an SM protein that is a component of the HOPS tethering complex, regulates vacuolar fusion pore expansion (Pieren et al., 2010). Our data offer tantalizing spatiotemporal evidence that a multisubunit tether might promote vesicle fusion; causal experiments are underway to validate this concept.

Materials and methods

Tissue cell culture, lentivirus generation, and reagents

HeLa and EA hy926 cells were cultured in DMEM (Invitrogen) with 10% FBS (Sigma-Aldrich) and supplemented with 500 µg/ml hygromicyn B (Invitrogen) for selection of shRNA and with 3 µg/ml puromycin (Sigma-Aldrich) for selection of rSec8-TagRFP stables. HEK293FT cells (Invitrogen) were cultured in DMEM and used for lentivirus production. In brief, HEK293FT cells were transfected with 2 µg of shRNA or cDNA vectors, plus 1 µg psPAX2 (Addgene) and 1 µg pMD2.G (Addgene) using Lipofectamine 2000 (Invitrogen). After overnight incubation, the medium was replaced and cells were grown for 48 h. Medium was recovered and centrifuged for 15 min at 1,000 *g* to remove cells debris. Supernatant was mixed at a 3:1 ratio with Lenti-X concentrator (Takara Bio Inc.) to precipitate and concentrate the virus particles. Particles were resuspended with 500 µl PBS and 100–150 µl were used to infect cells in the presence of 10 µg/ml polybrene. The next day, medium was replaced and cells were incubated for 24 h before adding medium with hygromicyn B of puromycin for selection. In the case of Sec8KD/rSec8-TagRFP double infected cells, the Sec8 shRNA stable cells were generated first, followed by rSec8-TagRFP infection.

Antibodies used were as follow: Sec8 (mouse monoclonal; M. Caplan, Yale University, New Haven, CT), GAPDH (rabbit polyclonal; New England Biolabs, Inc.), TagRFP (rabbit polyclonal; Evrogen), Exo70 (mouse monoclonal; S. Hsu, Rutgers University, New Brunswick, NJ), Sec5 (mouse monoclonal; A. Saltiel, University of Michigan, Ann Arbor, MI), and Sec6 (mouse monoclonal; M. Caplan).

Transient KD and replacement experiments for Sec8 were done using a 19-nucleotide RNAi sequence: 5′-CCUUGAUACCUCUCACUAU-3′ (Invitrogen). Transient transfection of HeLa cells with 100 nM RNAi was done with Lipofectamine RNAiMAX reagent using the reverse transfection protocol (Invitrogen) with Medium GC scramble RNAi control sequence as a negative control. The next day, cells were washed with DMEM and transiently transfected with 0.6–1 µg of plasmids expressing rSec8-TagRFP or other cargos (e.g., Vamp2-GFP or Vamp2-pHluorin) using Fugene HD transfection reagent (Promega). Cells were incubated for 36 h to account for 60 h of RNAi treatment before imaging.

Cloning of shRNA and plasmids constructs

Lentivirus production plasmids pLKO-scrambled (scram), pLKO-hyg, psPAX2, and pMD2.G were obtained from Addgene. The Addgene protocol to clone shRNA into plKO-hyg plasmid was followed. In brief, Sec8 shRNA primers 5′-CCGGATAGTGAGAGGTATCAAGGCTCGAGCCTTGATACCTCTCACTATTTTTTG-3′ and 5′-AATTCAAAAAATAGTGAGAGGTATCAAGGCTCGAGCCTTGATACCTCTCACTAT-3′ were annealed and cloned into pLKO-hyg, which was cut with EcoRI and AgeI restriction enzymes. Positive clones were analyzed by sequencing to validate Sec8 shRNA cloning. To generate pLVX-puro-rSec8-TagRFP lentivirus vector, first the rat Sec8 cDNA was cloned into pmTagRFP-T-N1 vector (provided by M. Davidson, Florida State Univeristy, Tallahassee, FL) as a XhoI–KpnI fragment to generate rSec8-TagRFP. After sequencing and expression validation the rSec8-TagRFP fragment was cut as a XhoI–NotI and subcloned into pLVX-puro plasmid in which a NotI site was added to the 3′ end of the multiple cloning site (Takara Bio Inc.). The ssFM4-pHluorin construct was generated by replacing the 5′SpeI-FCS-hGH-3′BamHI fragment on pC4S1-FM4-FCS-hGH (Jaiswal et al., 2009) with a 5′SpeI-pHluorin-3′BamHI PCR fragment amplified from Vamp2-pHluorin plasmid (J. Rothman, Yale University). To generate TfRcFM4-phluorin, the signal sequence from ssFM4-phluorin was replaced by 5′EcoRI-TfRc-3′XbaI PCR fragment amplified from TFRc-pHluorin plasmid.

Exocyst IP

Stable HeLa Scram and Sec8KD/rSec8-TagRFP were used for these experiments. For each cell line, two 10-cm dishes were prepared at 60–80% confluency. Dishes were transferred to a cold-room and cells were washed twice with 25 mM Tris-HCl, pH 6.8, 20 mM NaN_3, and 20 mM NaF. Cell lysis was done by treatment for 5 min with IP lysis buffer (25 mM Tris-HCl, pH 6.8, 150 mM NaCl, 1 mM EDTA, 1% Tween 20, 20 mM NaN_3, 20 mM NaF, 100 mM PMSF, and protease inhibitor cocktail [Roche]). Cells were scraped from the dishes and transferred to 1.5-ml eppendorf tubes. The lysates were passed through a 25-gauge syringe 10 times. To clear the lysates the samples were centrifuged for 10 min at 10,000 *g* at 4°C. Supernatants were recovered and 750–800 µl were used for IP. The IP samples were precleared for 1 h at 4°C with 30 µl of 50% Protein A agarose beads that were prewashed with lysis buffer. After centrifugation at 600 *g* the supernatants were incubated with 3 µg of rabbit polyclonal against TagRFP (Evrogen) overnight with constant rotation at 4°C. To isolate the complex, 40 µl of 50% Protein A agarose beads were added and incubated for 1 h. Samples were centrifuge at 600 *g* for 5 min and beads were washed four times with 750 µl of cold lysis buffer. The beads were then resuspended with 30 µl of lysis buffer and 30 µl of 2× loading buffer and boiled for 5 min to elute the proteins from the beads. For Western blot analysis, 2% of total lysate and 20% of the IP samples were run side by side on a 10% SDS-PAGE and visualized using a west-pico chemiluminescent substrate kit (Thermo Fisher Scientific) as per the manufacturer's recommendations.

Live-cell imaging and analysis

TIRFM was done as described previously (Xu et al., 2011) using a microscope (IX-70; Olympus) equipped with argon (488 nm) and argon/krypton (568 nm) laser lines, a TIRFM condenser (Olympus or custom condenser), a 60× 1.45 NA TIRF objective (Olympus), and an EMCCD camera (iXon887; Andor Technology) and controlled using iQ software (Andor Technology). All live-cell microscopy was done at 37°C (using a custom incubation chamber) in phenol red–free DMEM with 10% FCS and 25 mM Hepes, pH 7.4. Calibration of the evanescent field penetration depth was done using ∼20-µm silica beads coated with fluorescent rhodamine dye as a reference object of known geometry (Mattheyses and Axelrod, 2006; Xu et al., 2011; the exact bead diameter was determined by taking a z stack using a PIFOC piezo device [Physik Instrumente]). TIRFM/FRAP experiments were performed in a TIRF microscope capable of switching from a TIRF light path to wide-field point-scanning FRAP illumination using a pair of xy Galvo mirrors. The Galvo mirrors selectively steer the light beam between two light paths, which have a different number of lenses, so as to generate a collimated (FRAP) or focused beam (TIRF) at the back focal plane of the objective (these are combined by a 50/50 dichroic or custom partially mirrored surface). This microscope was equipped with 405-, 488-, and 568-nm lasers and a similar EMCCD camera and a 60× 1.49 NA TIRF objective (Olympus).

For TIRF/FRAP experiments cells were imaged by TIRF for 120 s at 1 Hz (150 Fms exposure/frame) using 568-nm illumination. On-the-fly photobleaching was done by 1 s of high speed, region of interest (ROI) scanning, using in-house C++ control software (developed by V. Polejaev, Yale University); after photobleaching cells were immediately imaged for 300 s by TIRFM at the initial acquisition conditions. Intensity changes of the ROI before and after FRAP were analyzed using ImageJ (the intensities were normalized to the maximum intensity peak before FRAP to determine the kinetics of recovery). Long time-lapse imaging of stable EA hy926 Sec8KD/rSec8-TagRFP transfected with TfRc-pH were obtained by a TIRFM at 37°C as described in Xu et al. (2011). The rSec8-TagRFP and TfRc-pH images were acquired sequentially with 650-ms exposure every 30 s for 45 min.

Analysis of pHluorin-tagged vesicle fusion was done as described previously (Xu et al., 2011), and the intensity of Sec8-TagRFP particle duration was analyzed using Volocity software (PerkinElmer). Specifically, stacks of images representing horizontal line kymographs of rSec8-TagRFP–expressing cell were generated and loaded into Volocity, and rSec8-TagRFP object "tracks" were selected based on their intensities; the duration of the tracks was measured by determining the length of the selected tracks in pixels and multiplying it by 500 ms, which represents the two frames per second acquisition rate used.

For improved presentation, in all figures and supplemental movies the raw microscopy data were Gaussian blurred (0.75 pixels) in ImageJ. To generate Quicktime movies the raw TIFF files were compressed sixfold (this introduces some high frequency pattern noise not present in the original data). Only linear adjustments were made to the brightness and contrast.

Online supplemental material

Fig. S1 shows colocalization of rSec8-TagRFP puncta with Vamp2-GFP in curvilinear tracks around the perinuclear region of cells and the shows changes in rSec8-TagRFP intensity relative to Vamp2-GFP vesicles. Fig. S2 shows images and quantification of the observed increase in accumulation of Tf-Alexa568 at the perinuclear region in HeLa Sec8KD stables when compared with HeLa control (scramble) cell and how this phenotype is rescued in HeLa Sec8KD rSec8-TagRFP. Fig. S3 shows the levels of Sec8KD and rSec8-TagRFP obtained in EA hy926 stable cell lines. Video 1 shows localization of rSec8-TagRFP after KD of endogenous Sec8 in a HeLa cell. Video 2 shows dual color TIRFM of rSec8-TagRFP and Vamp2-GFP. Video 3 shows dual color TIRFM of rSec8-TagRFP and Vamp2-pHluorin. Video 4 shows TIRFM/FRAP analysis of rSec8-TagRFP in membrane protrusion. Video 5 shows dual color TIRFM of rSec8-TagRFP and TfRc-pH during cell migration. Online supplemental material is available at http://www.jcb.org/cgi/content/full/jcb.201212103/DC1.

We thank Seong An, John Goss, and Martin Schwartz for comments on the manuscript. We thank John Lazar, Brian McNellis, and Emil Kromann for assistance with analysis and Vladimir Polejaev for assistance with TIRFM/FRAP instrumentation at the Yale CINEMA imaging center.

This research was supported through grants to D. Toomre from the National Institutes of Health (New Innovator Award 1DP2OD002980), the Yale Cancer Center Grant, and the Wellcome Trust Foundation.

Submitted: 19 December 2012
Accepted: 11 April 2013

References

Andersen, N.J., and C. Yeaman. 2010. Sec3-containing exocyst complex is required for desmosome assembly in mammalian epithelial cells. *Mol. Biol. Cell*. 21:152–164. http://dx.doi.org/10.1091/mbc.E09-06-0459

Ang, A.L., T. Taguchi, S. Francis, H. Fölsch, L.J. Murrells, M. Pypaert, G. Warren, and I. Mellman. 2004. Recycling endosomes can serve as intermediates during transport from the Golgi to the plasma membrane of MDCK cells. *J. Cell Biol.* 167:531–543. http://dx.doi.org/10.1083/jcb.200408165

Bendezú, F.O., and S.G. Martin. 2011. Actin cables and the exocyst form two independent morphogenesis pathways in the fission yeast. *Mol. Biol. Cell*. 22:44–53. http://dx.doi.org/10.1091/mbc.E10-08-0720

Bendezú, F.O., V. Vincenzetti, and S.G. Martin. 2012. Fission yeast Sec3 and Exo70 are transported on actin cables and localize the exocyst complex to cell poles. *PLoS ONE*. 7:e40248. http://dx.doi.org/10.1371/journal.pone.0040248

Boyd, C., T. Hughes, M. Pypaert, and P. Novick. 2004. Vesicles carry most exocyst subunits to exocytic sites marked by the remaining two subunits, Sec3p and Exo70p. *J. Cell Biol.* 167:889–901. http://dx.doi.org/10.1083/jcb.200408124

Bröcker, C., S. Engelbrecht-Vandré, and C. Ungermann. 2010. Multisubunit tethering complexes and their role in membrane fusion. *Curr. Biol.* 20:R943–R952. http://dx.doi.org/10.1016/j.cub.2010.09.015

Cai, H., S. Yu, S. Menon, Y. Cai, D. Lazarova, C. Fu, K. Reinisch, J.C. Hay, and S. Ferro-Novick. 2007. TRAPPI tethers COPII vesicles by binding the coat subunit Sec23. *Nature*. 445:941–944. http://dx.doi.org/10.1038/nature05527

Essid, M., N. Gopaldass, K. Yoshida, C. Merrifield, and T. Soldati. 2012. Rab8a regulates the exocyst-mediated kiss-and-run discharge of the *Dictyostelium* contractile vacuole. *Mol. Biol. Cell*. 23:1267–1282. http://dx.doi.org/10.1091/mbc.E11-06-0576

Finger, F.P., T.E. Hughes, and P. Novick. 1998. Sec3p is a spatial landmark for polarized secretion in budding yeast. *Cell*. 92:559–571. http://dx.doi.org/10.1016/S0092-8674(00)80948-4

Fölsch, H., M. Pypaert, S. Maday, L. Pelletier, and I. Mellman. 2003. The AP-1A and AP-1B clathrin adaptor complexes define biochemically and functionally distinct membrane domains. *J. Cell Biol.* 163:351–362. http://dx.doi.org/10.1083/jcb.200309020

Grindstaff, K.K., C. Yeaman, N. Anandasabapathy, S.C. Hsu, E. Rodriguez-Boulan, R.H. Scheller, and W.J. Nelson. 1998. Sec6/8 complex is recruited to cell-cell contacts and specifies transport vesicle delivery to the basal-lateral membrane in epithelial cells. *Cell*. 93:731–740. http://dx.doi.org/10.1016/S0092-8674(00)81435-X

Grosshans, B.L., A. Andreeva, A. Gangar, S. Niessen, J.R. Yates III, P. Brennwald, and P. Novick. 2006. The yeast lgl family member Sro7p is an effector of the secretory Rab GTPase Sec4p. *J. Cell Biol.* 172:55–66. http://dx.doi.org/10.1083/jcb.200510016

Guichard, A., S.M. McGillivray, B. Cruz-Moreno, N.M. van Sorge, V. Nizet, and E. Bier. 2010. Anthrax toxins cooperatively inhibit endocytic recycling by the Rab11/Sec15 exocyst. *Nature*. 467:854–858. http://dx.doi.org/10.1038/nature09446

He, B., and W. Guo. 2009. The exocyst complex in polarized exocytosis. *Curr. Opin. Cell Biol.* 21:537–542. http://dx.doi.org/10.1016/j.ceb.2009.04.007

Heider, M.R., and M. Munson. 2012. Exorcising the exocyst complex. *Traffic*. 13:898–907. http://dx.doi.org/10.1111/j.1600-0854.2012.01353.x

Hsu, S.C., C.D. Hazuka, R. Roth, D.L. Foletti, J. Heuser, and R.H. Scheller. 1998. Subunit composition, protein interactions, and structures of the mammalian brain sec6/8 complex and septin filaments. *Neuron*. 20:1111–1122. http://dx.doi.org/10.1016/S0896-6273(00)80493-6

Jaiswal, J.K., V.M. Rivera, and S.M. Simon. 2009. Exocytosis of post-Golgi vesicles is regulated by components of the endocytic machinery. *Cell*. 137:1308–1319. http://dx.doi.org/10.1016/j.cell.2009.04.064

Kanzaki, M., and J.E. Pessin. 2003. Insulin signaling: GLUT4 vesicles exit via the exocyst. *Curr. Biol.* 13:R574–R576. http://dx.doi.org/10.1016/S0960-9822(03)00478-0

Langevin, J., M.J. Morgan, J.B. Sibarita, S. Aresta, M. Murthy, T. Schwarz, J. Camonis, and Y. Bellaïche. 2005. *Drosophila* exocyst components Sec5, Sec6, and Sec15 regulate DE-Cadherin trafficking from recycling endosomes to the plasma membrane. *Dev. Cell*. 9:365–376. http://dx.doi.org/10.1016/j.devcel.2005.07.013

Lees, J.A., C.K. Yip, T. Walz, and F.M. Hughson. 2010. Molecular organization of the COG vesicle tethering complex. *Nat. Struct. Mol. Biol.* 17:1292–1297. http://dx.doi.org/10.1038/nsmb.1917

Letinic, K., R. Sebastian, D. Toomre, and P. Rakic. 2009. Exocyst is involved in polarized cell migration and cerebral cortical development. *Proc. Natl. Acad. Sci. USA*. 106:11342–11347. http://dx.doi.org/10.1073/pnas.0904244106

Liu, J., and W. Guo. 2012. The exocyst complex in exocytosis and cell migration. *Protoplasma*. 249:587–597. http://dx.doi.org/10.1007/s00709-011-0330-1

Matern, H.T., C. Yeaman, W.J. Nelson, and R.H. Scheller. 2001. The Sec6/8 complex in mammalian cells: characterization of mammalian Sec3, subunit interactions, and expression of subunits in polarized cells. *Proc. Natl. Acad. Sci. USA*. 98:9648–9653. http://dx.doi.org/10.1073/pnas.171317898

Mattheyses, A.L., and D. Axelrod. 2006. Direct measurement of the evanescent field profile produced by objective-based total internal reflection fluorescence. *J. Biomed. Opt.* 11:014006. http://dx.doi.org/10.1117/1.2161018

Morgera, F., M.R. Sallah, M.L. Dubuke, P. Gandhi, D.N. Brewer, C.M. Carr, and M. Munson. 2012. Regulation of exocytosis by the exocyst subunit Sec6 and the SM protein Sec1. *Mol. Biol. Cell*. 23:337–346. http://dx.doi.org/10.1091/mbc.E11-08-0670

Moskalenko, S., C. Tong, C. Rosse, G. Mirey, E. Formstecher, L. Daviet, J. Camonis, and M.A. White. 2003. Ral GTPases regulate exocyst assembly through dual subunit interactions. *J. Biol. Chem.* 278:51743–51748. http://dx.doi.org/10.1074/jbc.M308702200

Munson, M., and P. Novick. 2006. The exocyst defrocked, a framework of rods revealed. *Nat. Struct. Mol. Biol.* 13:577–581. http://dx.doi.org/10.1038/nsmb1097

Novick, P., C. Field, and R. Schekman. 1980. Identification of 23 complementation groups required for post-translational events in the yeast secretory pathway. *Cell*. 21:205–215. http://dx.doi.org/10.1016/0092-8674(80)90128-2

Oztan, A., M. Silvis, O.A. Weisz, N.A. Bradbury, S.C. Hsu, J.R. Goldenring, C. Yeaman, and G. Apodaca. 2007. Exocyst requirement for endocytic traffic directed toward the apical and basolateral poles of polarized MDCK cells. *Mol. Biol. Cell*. 18:3978–3992. http://dx.doi.org/10.1091/mbc.E07-02-0097

Pecenková, T., M. Hála, I. Kulich, D. Kocourková, E. Drdová, M. Fendrych, H. Toupalová, and V. Zársky. 2011. The role for the exocyst complex subunits Exo70B2 and Exo70H1 in the plant-pathogen interaction. *J. Exp. Bot.* 62:2107–2116. http://dx.doi.org/10.1093/jxb/erq402

Pieren, M., A. Schmidt, and A. Mayer. 2010. The SM protein Vps33 and the t-SNARE H(abc) domain promote fusion pore opening. *Nat. Struct. Mol. Biol.* 17:710–717. http://dx.doi.org/10.1038/nsmb.1809

Prigent, M., T. Dubois, G. Raposo, V. Derrien, D. Tenza, C. Rossé, J. Camonis, and P. Chavrier. 2003. ARF6 controls post-endocytic recycling through its downstream exocyst complex effector. *J. Cell Biol.* 163:1111–1121. http://dx.doi.org/10.1083/jcb.200305029

Rivera, V.M., X. Wang, S. Wardwell, N.L. Courage, A. Volchuk, T. Keenan, D.A. Holt, M. Gilman, L. Orci, F. Cerasoli Jr., et al. 2000. Regulation of protein secretion through controlled aggregation in the endoplasmic reticulum. *Science*. 287:826–830. http://dx.doi.org/10.1126/science.287.5454.826

Rossé, C., A. Hatzoglou, M.C. Parrini, M.A. White, P. Chavrier, and J. Camonis. 2006. RalB mobilizes the exocyst to drive cell migration. *Mol. Cell. Biol.* 26:727–734. http://dx.doi.org/10.1128/MCB.26.2.727-734.2006

Rosse, C., E. Formstecher, K. Boeckeler, Y. Zhao, J. Kremerskothen, M.D. White, J.H. Camonis, and P.J. Parker. 2009. An aPKC-exocyst complex controls paxillin phosphorylation and migration through localised JNK1 activation. *PLoS Biol.* 7:e1000235. http://dx.doi.org/10.1371/journal.pbio.1000235

Sivaram, M.V., J.A. Saporita, M.L. Furgason, A.J. Boettcher, and M. Munson. 2005. Dimerization of the exocyst protein Sec6p and its interaction with the t-SNARE Sec9p. *Biochemistry*. 44:6302–6311. http://dx.doi.org/10.1021/bi048008z

Stroupe, C., C.M. Hickey, J. Mima, A.S. Burfeind, and W. Wickner. 2009. Minimal membrane docking requirements revealed by reconstitution of Rab GTPase-dependent membrane fusion from purified components. *Proc. Natl. Acad. Sci. USA*. 106:17626–17633. http://dx.doi.org/10.1073/pnas.0903801106

Sztul, E., and V. Lupashin. 2009. Role of vesicle tethering factors in the ER-Golgi membrane traffic. *FEBS Lett.* 583:3770–3783. http://dx.doi.org/10.1016/j.febslet.2009.10.083

TerBush, D.R., T. Maurice, D. Roth, and P. Novick. 1996. The Exocyst is a multiprotein complex required for exocytosis in *Saccharomyces cerevisiae*. *EMBO J.* 15:6483–6494.

Vardjan, N., J. Jorgacevski, and R. Zorec. 2013. Fusion pores, SNAREs, and exocytosis. *Neuroscientist*. 19:160–174. http://dx.doi.org/10.1177/1073858412461691

Wiederkehr, A., J.O. De Craene, S. Ferro-Novick, and P. Novick. 2004. Functional specialization within a vesicle tethering complex: bypass of a subset of exocyst deletion mutants by Sec1p or Sec4p. *J. Cell Biol.* 167:875–887. http://dx.doi.org/10.1083/jcb.200408001

Wu, H., G. Rossi, and P. Brennwald. 2008. The ghost in the machine: small GTPases as spatial regulators of exocytosis. *Trends Cell Biol.* 18:397–404. http://dx.doi.org/10.1016/j.tcb.2008.06.007

Xu, Y., B.R. Rubin, C.M. Orme, A. Karpikov, C. Yu, J.S. Bogan, and D.K. Toomre. 2011. Dual-mode of insulin action controls GLUT4 vesicle exocytosis. *J. Cell Biol.* 193:643–653. http://dx.doi.org/10.1083/jcb.201008135

Yu, I.M., and F.M. Hughson. 2010. Tethering factors as organizers of intracellular vesicular traffic. *Annu. Rev. Cell Dev. Biol.* 26:137–156. http://dx.doi.org/10.1146/annurev.cellbio.042308.113327

Zárský, V., and M. Potocký. 2010. Recycling domains in plant cell morphogenesis: small GTPase effectors, plasma membrane signalling and the exocyst. *Biochem. Soc. Trans.* 38:723–728. http://dx.doi.org/10.1042/BST0380723